

Title: Mg-sursassite thermo-elastic parameters and its relevance as a water carrier in subducting slabs

Manuscript Number: 8034R

Authors: Sula Milani, University of Milan Patrizia Fumagalli, Università di Milano Juliette Maurice, Università degli Studi di Milano Paolo Lotti, Università degli Studi di Milano Davide Comboni, European Synchrotron Radiation Facility Francesco Pagliaro, Università degli Studi di Milano Michael Hanfland, ESRF Giorgio Bais, Elettra Sincrotrone Trieste Bobby Joseph, Elettra Sincrotrone Trieste Marco Merlini, Università degli Studi di Milano

1 Revision 1

2 Mg-sursassite thermo-elastic parameters and its relevance as a water carrier in  
3 subducting slabs

4

5 Milani Sula<sup>1</sup>, Fumagalli Patrizia<sup>1</sup>, Luca Ziberna<sup>2</sup>, Maurice Juliette<sup>1</sup>, Lotti Paolo<sup>1</sup>, Comboni Davide<sup>1,3</sup>,  
6 Pagliaro Francesco<sup>1</sup>, Hanfland Michael<sup>3</sup>, Bais Giorgio<sup>4</sup>, Joseph Boby<sup>4</sup>, Merlini Marco<sup>1</sup>

7 <sup>1</sup> Dipartimento di Scienze della Terra ‘Ardito Desio’, Università degli Studi di Milano, via Botticelli  
8 23, 20133, Milan, Italy

9 <sup>2</sup> Dipartimento di Matematica e Geoscienze, Università degli Studi di Trieste, via Weiss 8, 34128,  
10 Trieste, Italy

11 <sup>3</sup> ESRF-European Synchrotron Radiation Facility, 71 Avenue des Martyrs, CS40220, Grenoble Cedex,  
12 38043, France

13 <sup>4</sup> Elettra-Sincrotrone Trieste S.C.p. A., Strada Statale 14 km 163.5, Basovizza, Trieste, 34149, Italy

#### 14 **Abstract**

15 We report the synthesis, at 7 GPa and 923 K, and the thermoelastic characterization, up to 16 GPa and  
16 850 K, of single crystal of Mg-sursassite,  $\text{Mg}_5\text{Al}_5\text{Si}_6\text{O}_{21}(\text{OH})_7$ . In-situ high-pressure and high-  
17 temperature single crystal diffraction allowed the study of structural variation at non-ambient conditions  
18 and the determination of bulk elastic properties. The refined parameters of a second order Birch-  
19 Murnaghan Equation of State (BM-II EoS) are  $V_0 = 446.02(1) \text{ \AA}^3$  and  $K_{T0} = 135.6(7) \text{ GPa}$ . The thermal  
20 expansion coefficients of a Berman-type EoS are  $\alpha_0 = 3.14(5) \times 10^{-5} \text{ K}^{-1}$ ,  $\alpha_1 = 2.50(16) \times 10^{-8} \text{ K}^{-2}$  and  
21  $V_0 = 445.94(3)$ . For comparison, the  $P$ - $V$  Equation of State is determined for a natural sursassite sample,  
22 ideally  $\text{Mn}_4\text{Al}_6\text{Si}_6\text{O}_{22}(\text{OH})_6$ . The refined parameters of BM-II EoS ( $V_0 = 470.2(3) \text{ \AA}^3$ ,  $K_{T0} = 128(4) \text{ GPa}$ )  
23 indicate that composition has a minimal effect on elastic properties. The similarity of density and bulk  
24 properties of Mg-sursassite if compared to olivine and other anhydrous mantle minerals suggests that  
25 this phase could be overseen by geophysical methods.

26 **Keywords:** Mg-sursassite, hydrous minerals, structure, thermo-elastic parameters.

#### 27 **1. Introduction**

28 The deep-water cycle plays a fundamental role in the evolution of Earth and has a strong influence on  
29 life creation and sustainability. High-pressure and high-temperature experimental petrology shows that  
30 the number of possible hydrous phases that can carry water into the Earth's mantle via subduction is  
31 quite broad. The determination of the stability field of these hydrous phases and of the mechanism of  
32 sequestration and release of water accomplished through their occurrence are paramount to unravel the  
33 evolution of our 'water' planet. Mg-sursassite is one of these hydrates. This phase has been first  
34 synthesized in the simple MgO-Al<sub>2</sub>O<sub>3</sub>-SiO<sub>2</sub>-H<sub>2</sub>O (MASH) system with either a Ca-free or MgMg-Al  
35 pumpellyite structure (Schreyer et al. 1986; Fockenberg 1998) or in a disordered pumpellyite structure  
36 with local sursassite-type geometry (Artioli et al. 1999). Its crystal structure has been further constrained  
37 using Rietveld method and transmission electron microscopy to an isostructural arrangement as Mn-  
38 sursassite Mn<sub>4</sub>Al<sub>2</sub>Al<sub>4</sub>Si<sub>6</sub>O<sub>22</sub>(OH)<sub>6</sub>. In this, Mn to Mg substitution takes place together with Al  
39 replacement by Mg + H, thus giving a nominal chemical formula of Mg<sub>5</sub>Al<sub>5</sub>Si<sub>6</sub>O<sub>21</sub>(OH)<sub>7</sub> and hence has  
40 been referred as Mg-sursassite (Gottschalk et al. 2000).

41 Mg-sursassite is a sorosilicate mineral, that forms after the breakdown of layered minerals like chlorite  
42 and retains water in its structure. It belongs to the group of 'Dense Hydrous Magnesium-Aluminum  
43 Silicates' (DHMAS). As the majority of DHMAS and Dense Hydrous Magnesium Silicates' (DHMS),  
44 Mg-sursassite is characterised by a modulated-layered structure. The main characteristic of  
45 DHMS/DHMAS is that they are stable and they can bear a large amount of 'water' (e.g. phase E can hold  
46 up to 18wt% of H<sub>2</sub>O) even under extreme conditions,  $P = 13-18$  GPa and  $T = 1573$  K (Purevjav et al.  
47 2020 and references therein). Indeed, they represent the major group of minerals which have a large  
48 hydrogen storage capacity over a wide pressure and temperature range (Purevjav et al. 2020),  
49 contributing therefore to the global water budget, which is one of the key topics for understanding the  
50 nature and evolution of the Earth's interior, since water can affect mantle rheology, melting temperature  
51 and electrical conductivity (e.g. Smyth 2006).

52 It has been already demonstrated that Mg-sursassite ( $\text{Mg}_5\text{Al}_5\text{Si}_6\text{O}_{21}(\text{OH})_7$ ), containing about 7 wt%  $\text{H}_2\text{O}$ ,  
53 can be a possible high-pressure carrier of significant volumes of  $\text{H}_2\text{O}$  in a range of bulk compositions  
54 from pelitic (Domanik and Holloway 1996) to mafic/ultramafic compositions (Fockenberg 1998; Artioli  
55 et al. 1999, Bromiley and Pawley 2002). Indeed, its stability field was originally defined in the interval  
56 6–7 GPa and  $< 973$  K, allowing water transfer in the subducting slab from chlorite minerals to the high  
57 pressure dense hydrous magnesium silicate phase A. For instance, a chlorite-bearing peridotite  
58 containing 2.8 wt%  $\text{H}_2\text{O}$  could provide the transfer of 0.98 wt%  $\text{H}_2\text{O}$  via the reaction  
59 chlorite+enstatite=Mg-sursassite+forsterite+fluid (Luth 2003). Recently, a Si-rich Mg-sursassite with  
60 octahedrally coordinated Si (Bindi et al. 2020), has brought more attention to this phase, because it was  
61 synthesized at more extreme conditions of 24 GPa and 1673 K, broadening the stability field of this phase  
62 and casting new light on the fate of this phase in cold subducting slabs.

63 Recently, other new hydrous high-pressure phases in the MASH system were identified at mantle  
64 conditions (Fumagalli et al. 2014; Cai et al. 2015; Gemmi et al. 2016) as candidate water carriers in deep  
65  $\text{H}_2\text{O}$  cycle. It is unlikely to recover natural samples of these candidate minerals, therefore the  
66 determination of their physical and thermodynamic properties is the main means of understanding the  
67 possibility of indirectly identifying them through geophysical methods.

68 We have been successful in synthesising large Mg-sursassite crystals which permitted us to carry out  
69 structural characterizations with in-situ diffractometric techniques. In this paper we report the thermo-  
70 elastic and structural behaviour of Mg-sursassite at high-pressure or high-temperature, obtained by in-  
71 situ single crystal X-ray diffraction techniques at synchrotron radiation facilities, in relation with its  
72 mineral composition. The results will constitute a valuable experimental dataset, fundamental for any  
73 further study.

## 74 **2. Experimental methods**

75 Synthetic large single crystals (up to  $200 \times 100 \times 100 \mu\text{m}^3$ ) of Mg-sursassite were obtained at high pressure  
76 and high temperature using a multi-anvil module at the Department of Earth Sciences, University of  
77 Milan (DES-UM). A gel of stoichiometric composition, modelled in the MASH system, was used as a  
78 starting material prepared following the procedure adopted by Hamilton and Henderson (1968). Platinum  
79 capsules (3.5 mm length and 2 mm diameter) were welded after being loaded with the gel and saturated  
80 with water, which was added with a micro-syringe. Cr-doped MgO octahedra of 25 mm of edge length  
81 were used as pressure cell in 32 mm edge length tungsten carbide cubes. Graphite heaters were used, and  
82 temperatures were measured by a Pt-PtRh thermocouple (S-type). Temperature is accurate to  $\pm 20$  K,  
83 with no pressure correction for e.f.m. of thermocouple. Pressure uncertainties were assumed  $\pm 3\%$   
84 according to the accuracy of calibrant reactions (Fumagalli and Poli 2005). Samples of Mg-sursassite  
85 were synthesized at 7 GPa and 923 K (ramp rate at about 35 K/min) with a run duration of 72 hours. The  
86 multi-anvil experiment was performed with a Cr-doped MgO octahedron of 25 mm edge length  
87 combined with tungsten carbide cubes of 15 mm truncation-edge lengths. For the experiment a graphite  
88 heater was employed. All the minerals were characterized via preliminary single crystal X-ray diffraction  
89 measurements. Mineral composition of selected Mg-sursassite crystals was determined via electron  
90 microprobe analysis (EMPA) at the DES-UM using a Jeol 8200 electron microprobe operating at 15 nA  
91 and 15 kV, with standard of pyrope for both Si and Mg.

92 A synthetic single crystal of Mg-sursassite ( $\sim 60 \times 50 \times 15 \mu\text{m}^3$ ) was picked from the experimental charge  
93 and glued on a glass fiber, which was attached on a metallic pin. The single-crystal x-ray diffraction  
94 measurement was carried out at the DES-UM at room temperature using a four circles  $\kappa$ -geometry Rigaku  
95 XtaLAB Synergy diffractometer equipped with a PhotonJet (Mo) X-ray Source, operating at 50 kV and  
96 1 mA, with a monochromatized  $\text{MoK}\alpha$  radiation, and with a Hybrid Pixel Array detector at 150 mm from  
97 the sample position. The measurement strategy was programmed with a combination of scans in  $\omega$  with

98 0.5° step and with an exposure time of 3.5 s at each scan step for different  $2\theta$ ,  $\kappa$  and  $\phi$  positions. Data  
99 reductions, including Lorenz-polarization and absorption correction based on the implemented semi-  
100 empirical ABSPACK routine, were performed using the software CrysAlisPro (Rigaku Oxford  
101 Diffraction 2019).

102 For comparison, a natural sample of sursassite single crystal  
103  $(\text{Mn}^{2+}_{1.61}\text{Ca}_{0.39})_{\Sigma 2}(\text{Mn}_{0.25}\text{Al}_{2.33}\text{Mg}_{0.33}\text{Fe}^{3+}_{0.01})_{\Sigma 2.92}\text{Si}_{3.08}\text{O}_{10.49-10.74}(\text{OH})_{3.26-3.51}$  from La Falotta  
104 (Switzerland), kindly provided by the Museum of Mineralogy at the DES-UM, was also studied. We  
105 assume the chemical composition reported in Nagashima et al. (2009) for this natural sample. This natural  
106 crystal was selected for the absence of pumpelleyite domains in these samples (Nagashima et al. 2009)  
107 and for the possibility to pick up a single crystal of suitable size for high-pressure studies.

108 In-situ high-pressure (HP) single crystal X-ray diffraction measurements have been carried out at the  
109 beamline ID15b of the European Synchrotron Radiation Facility (ESRF, Grenoble), loading a synthetic  
110 single crystal of Mg-sursassite in a Diamon-Anvil Cell (DAC). The standard HP single crystal diffraction  
111 setup was used (Merlini and Hanfland 2013). Wavelength was 0.41130 Å. The pressure transmitting  
112 medium used in this experiment was neon, which transmits pressure hydrostatically up to the maximum  
113 pressure reached in this study of about ca. 16 GPa (Klotz et al. 2009). The HP experiment on the natural  
114 sursassite was instead performed at the Italian Synchrotron (Elettra, Trieste) HP beamline Xpress (Lotti  
115 et al. 2020) up to ca. 6 GPa. Wavelength was 0.49450 Å and the detector used was a MAR345 imaging  
116 plate. For this experiment the pressure transmitting medium was a 4:1 methanol:ethanol mixture, which  
117 transmits pressure hydrostatically up to the pressure reached in this measurement (Klotz et al. 2009). In  
118 both the experiments ruby fluorescence was used as a pressure standard (Mao et al. 1986; Chervin et al.  
119 2001).

120 In-situ high-temperature (HT) single crystal X-ray diffraction experiment was carried out at the XRD1  
121 beamline at the Italian Synchrotron (Elettra, Trieste). Wavelength was 0.7000 Å and the detector used  
122 was Pilatus 2M. A synthetic single crystal of Mg-sursassite, together with a single crystal of quartz used  
123 as standard, were loaded in a quartz-glass capillary and during the measurement crystals were kept steady  
124 with quartz-glass fibres. The data were collected every 30 K in a temperature range from 318 to 823 K.  
125 Temperature was maintained with a hot gas blower.

### 126 **3. Results and discussion**

#### 127 3.1 Crystal-chemical formula of Mg-sursassite

128 Ten data points were measured on a sample of Mg-sursassite by EMPA and the composition of the single  
129 point-analyses is shown in Table 1. The average empirical formula calculated from the ten analyses and  
130 based on 16 cations a.p.f.u. is  $\text{Mg}_{4.96(10)}\text{Al}_{4.93(8)}\text{Si}_{6.11(8)}\text{O}_{21.15}(\text{OH})_{6.85}$ . It is noticeable a slight excess of Si  
131 against nominal formula with six Si atoms a.p.f.u., which may occupy partially the smaller [6]-  
132 coordinated sites. The OH content is derived from charge balance.

#### 133 3.2 Crystal structure of Mg-sursassite

134 The single crystal X-ray diffraction measurements confirm that the structure is monoclinic. The refined  
135 unit cell from laboratory data is  $a = 8.5375 (16) \text{ \AA}$ ,  $b = 5.7097 (11) \text{ \AA}$ ;  $c = 9.6477 (17) \text{ \AA}$ ,  $\beta = 108.340$   
136  $(17)^\circ$  and  $V = 446.40 (15) \text{ \AA}^3$ . The structural refinement was handled via Jana2006 software (Petricek et  
137 al. 2014) starting from the atomic coordinates of a published crystal structure (Nagashima et al. 2009) in  
138 the space group  $P2_1/m$ . The Mg-sursassite is a sorosilicate characterized by layers of 6-coordinated sites  
139 (Fig.1a). As reported in Nagashima et al. (2009) the structure is characterized by two bigger 6-  
140 coordinated sites where the bivalent cation is located (Mg1 and Mg2), while the trivalent cation, Al,  
141 occupies the two smaller 6-coordinates sites (Al2, Al3). A further octahedral site has an intermediate  
142 volume if compared to  $\text{MgO}_6$  and  $\text{AlO}_6$  octahedra, and this site has likely a mixed Mg-Al occupancy  
143 (Fig. 1a). As it can be seen from the Fourier differences of the electron density (Fig. 1b) there are some

144 maxima close to O11, O7 and O6, where the H cations might be located, in agreement with literature  
145 data (Nagashima et al. 2009). The principal statistical parameters of the structure refinement are listed in  
146 Table 2. Atomic coordinates and site occupancies of structure refinements are given in Table S1.  
147 Anisotropic displacement parameters and relevant bond distances are reported in Table S2, S3. The  
148 crystallographic information file is available as Supplementary Materials.

### 149 3.3 Compressibility behavior of Mg- and natural sursassite

150 The evolution of the unit-cell volume of Mg-sursassite at different pressures is reported in Table 3. The  
151 volume decreases smoothly with increasing pressure, as shown in Fig. 2, up to the maximum hydrostatic  
152 conditions reached in this study of ca. 16 GPa. No phase transition or change of the deformation  
153 mechanisms occur within the *P*-range investigated. The *P*–*V* data were fitted using a second-order Birch–  
154 Murnaghan EoS (BM2-EoS; Birch 1947), since the Eulerian finite strain ( $f_e$ ) vs. normalized stress ( $F_e$ )  
155 plot ( $F_e$ – $f_e$  plot, Fig. S1a) of the data can be fitted by a horizontal straight line (Angel 2000). The BM2-  
156 EoS coefficients were refined simultaneously, data were weighted by their uncertainties in *P* and *V*, using  
157 the program EoSFit-7c (Angel et al. 2014) giving:  $V_0 = 446.1(1) \text{ \AA}^3$ ,  $K_{T0} = 135.6(7) \text{ GPa}$  and  $K' = 4$  fixed  
158 ( $\Delta P_{\text{max}} = -0.35 \text{ GPa}$ ,  $\chi^2_{\text{w}} = 1.92$ ). The calculated  $\Delta P_{\text{max}}$  and  $\chi^2_{\text{w}}$  values indicate that the EoS provide a  
159 good fit to the data.

160 Crystal structure refinements at variable pressures indicate that compression of the octahedral sites is  
161 function of their size, with the two Mg-sites more compressible than Al and (Al, Mg) sites. Silicon  
162 tetrahedral sites are much more incompressible (Fig. S2).

163 The unit-cell parameters of the natural sursassite decrease smoothly with increasing pressure to the  
164 maximum conditions reached in the experiment as shown in Fig. 3 and reported in Table S4. The  
165 experimental data were suitable only for lattice parameter determination. No phase transition or change  
166 of the deformation mechanisms occur within the *P*-range investigated (Fig.3). *P*-*V* data were fitted with



167 a BM2-EoS (Birch 1947), because the  $F_e-f_e$  plot (Fig. S1b) of the data can be fitted with a horizontal line  
168 (Angel 2000). As for the Mg-sursassite case, the BM2-EoS coefficients were refined simultaneously and  
169 the data were weighted by their uncertainties in  $P$  and  $V$  using the program EoSFit-7c (Angel et al. 2014).  
170 The so obtained coefficients are:  $V_0 = 470.2(3) \text{ \AA}^3$ ,  $K_{T0}=128(4) \text{ GPa}$  and  $K'=4$  fixed.

171 Note that the values of  $K_{T0}$  for natural and synthetic sursassite are the same within error, demonstrating  
172 no significant influence of composition on the value of the bulk modulus. Up to date only one study  
173 determined the bulk modulus of the Mg-sursassite (Grevel et al. 2001). This study has been carried out  
174 on a powder sample up to 7.52 GPa and the  $P$ - $V$  data are fitted with a BM2-EoS (Birch 1947) giving the  
175 following parameters:  $V_0 = 446.49 \text{ \AA}^3$ ,  $K_{T0}=116(1.3)$  and  $K'=4$ . The pressure transmitting medium in  
176 these experiments is vaseline, which is known not to transmit the pressure hydrostatically above 3 GPa  
177 (Tateiwa and Haga 2009), therefore the difference in the results could be due to a different experimental  
178 protocol.

### 179 3.4 Thermal expansion behavior of Mg-sursassite

180 The temperature ( $T$ ) – volume ( $V$ ) data collected during the experiment at ambient pressure are reported  
181 in Fig. 4 and Table 4. As it can be observed from Fig. 4,  $V$  increases continuously without any phase  
182 transition, any change of the deformation mechanisms or any evidence of an irreversible change in the  
183 crystal during the experiment up to the maximum  $T$  reached in the study. The  $V$ - $T$  data were fitted using  
184 EoSFit 7c (Angel et al. 2014) using a Berman-type EoS (Berman 1988). The thermal expansion  
185 coefficient obtained are:  $\alpha_0=3.14 (5) \times 10^{-5} \text{ K}^{-1}$ ,  $\alpha_1=2.50(16) \times 10^{-8} \text{ K}^{-2}$  and  $V_0=445.94(3)$  ( $\chi^2_w=1.34$ ).  
186 Data points 2, 3 and 16 were omitted in the fitting, due to an oscillation of the temperature during the  
187 data collection.

188 For sake of comparison between data presented in this study and those published by Grevel et al. (2001)  
189 data were re-fitted with a thermal pressure model (Holland and Powell 2011) using the program EoSFit-

190 7c (Angel et al. 2014). The Einstein temperature ( $\theta_E$ ) used to fit the data is 575.19 K. This value was  
191 estimated following Holland and Powell (2011), with entropy (S) taken from Grevel et al. (2001). The  
192 parameters obtained from the fitting are listed in Table 5. The main difference is visible in the value of  
193 the bulk-modulus of about 15 GPa (Table 5).

194 Single crystal structure refinements at variable temperatures reveal an inverse relationship of structural  
195 parameters (Hazen and Finger 1982) if compared to high-pressure data, with polyhedral volume  
196 expansion greater in Mg-octahedral sites than in Al-sites and a much lower expansion in tetrahedral sites  
197 (Fig. S3).

#### 198 **4. Implications and conclusions**

199 Synthesis of Mg-sursassite at 7 GPa and 923 K resulted in large prismatic single crystals up to  
200  $200 \times 100 \times 100 \mu\text{m}^3$ . Single crystal X-ray diffraction analysis indicates a pure sursassite structural model,  
201 without macroscopically detectable defects or intergrowths can well describe the data. It is worth noting  
202 that there is a slight excess of tetrahedrally coordinated Si, suggesting that the excess atoms are in the  
203 octahedral sites. The presence of octahedrally coordinated Si in Mg-sursassite has already been reported  
204 by Bindi et al. (2020), but their sample was synthesised at higher pressure and temperature (24 GPa and  
205 1673 K) with respect to our sample (7 GPa and 923 K). The presence of octahedrally coordinated Si in  
206 the sample synthesised in this study is in agreement with the so called majoritic substitution that occurs  
207 at pressures greater than  $\sim 5$  GPa and this represents the coupled substitution of Si and Mg (and Fe) onto  
208 the octahedrally coordinated site that occurs in garnets within mantle assemblages as a result of the  
209 breakdown of both orthopyroxene and clinopyroxene (Ringwood 1967).

210 Our HP diffraction study provides the bulk modulus of Mg-sursassite,  $K_{T0}$  to be 135.6(7) GPa. The  
211 obtained bulk modulus shows that its behaviour is stiffer with respect to DHMS such as phase A or phase  
212  $10\text{\AA}$  (Crichton and Ross 2000; Comodi et al. 2006), or if compared also to new high-pressure hydrous

213 phases in MASH system such as 11.5 Å, 23 Å and Hyso phase (Table 6). The compressibility of Mg-  
214 sursassite is comparable to forsterite and superhydrous phase B. Another important point worth of notice  
215 is that the values of the bulk moduli of synthetic Mg-sursassite and natural sursassite do not change  
216 significantly as function of composition implying that the effect of the composition variation on the  
217 elastic properties is almost irrelevant.

218 The thermoelastic values of Mg-sursassite extracted from this study might bear important implications  
219 about the detectability of this phase in the mantle by geophysical methods since these values are like the  
220 elastic parameters of nominally anhydrous mantle silicates. If we try to model the variation of the density  
221 ( $\text{g/cm}^3$ ) of the Mg-sursassite with respect to a  $\text{Mg}_2\text{SiO}_4$  (forsterite, fo) to 13 GPa (base of the upper  
222 mantle) we can observe that the difference is ca. of 1.15% (Fig. 5). If we assume that Mg-sursassite is a  
223 stable phase in the subducting slab down to the base of the upper mantle, this density difference might  
224 be too low to allow its detectability by geophysical methods from minerals like olivine (Fig. 5). In Fig.  
225 5 we can also observe how the values of the thermoelastic parameters determined in our study with  
226 respect to already published data influence the estimation of its density at upper mantle conditions.

227 Further studies are needed to constrain the properties and stability of Mg-sursassite and its possible solid  
228 solutions. This is because i) Mg-sursassite is a breakdown product of chlorite, which is considered the  
229 major water carrier at mantle depth in a cold slab subduction system (e.g. Fumagalli et al. 2014; Gemmi  
230 et al. 2016; Bromiley and Pawley 2002), ii) it can be stable up to pressures of the mantle transition zone  
231 (Bindi et al. 2020) and therefore may not be any longer only a link as a water carrier between the  
232 breakdown of the chlorite and the formation of phase A (Fumagalli et al., 2014; Bromiley and Pawley,  
233 2002), and iii) its elastic properties, comparable to those of nominally anhydrous mantle silicates, suggest  
234 that this phase can be overseen by geophysical methods.

## 235 **Acknowledgment**

236 European Synchrotron Radiation Facility is acknowledged for provision of beamtime at ID15B beamline.  
237 Elettra synchrotron facility is acknowledged for provision of beamtime at XPRESS and XRD1 beamline.  
238 The research leading to this result has been supported by the project CALIPSOplus under Grant  
239 Agreement 730872 from the EU Framework Programme for Research and Innovation HORIZON 2020.  
240 We acknowledge Andrea Risplendente for microprobe analysis and the “Museo delle Collezioni  
241 Mineralogiche” of the Earth Science department (Univ. Milano) for provision of natural sursassite  
242 sample. SM, PF, JM, PL, FP and MM acknowledge the support of the Italian Ministry of Education  
243 (MIUR) through the project “Dipartimenti di Eccellenza 2018–2022”. We are thankful to two anonymous  
244 reviewers for detailed and constructive comments, which helped to improve the manuscript substantially.

## 245 **References**

- 246 Angel, R.J. (2000) Equations of state. In R.M. Hazen and R.T. Downs, Eds., High-Temperature and  
247 High-Pressure Crystal Chemistry, 41, p 35-59. Reviews in Mineralogy and Geochemistry, Mineralogical  
248 Society of America, Chantilly, Virginia.
- 249 Angel, R.J., and Jackson, J.M. (2002) Elasticity and equation of state of orthoenstatite,  $\text{MgSiO}_3$ .  
250 *American Mineralogist*, 87, 558-561.
- 251 Angel, R.J., Gonzales-Platas, J., and Alvaro, M. (2014) EoSFit7c and a Fortran module (library) for  
252 equation of state calculations. *Zeitschrift für Kristallographie*, 229, 405-419.
- 253 Angel, R.J., Alvaro, M., and Nestola, F. (2018) 40 years of mineral elasticity: a critical review and a new  
254 parameterisation of equations of state for mantle olivines and diamond inclusions. *Physics and Chemistry  
255 of Minerals*, 45, 95-113.
- 256 Artioli, G., Fumagalli, P., and Poli, S. (1999). The crystal structure of  $\text{Mg}_8(\text{Mg}_2\text{Al}_2)\text{Al}_8\text{Si}_{12}(\text{O},\text{OH})_{56}$   
257 pumpellyite and its relevance in ultramafic systems at high pressure. *American Mineralogist*, 84, 1906-  
258 1914.

259 Berman, R.G. (1988) Internally-consistent thermodynamic data for minerals in the system Na<sub>2</sub>O-K<sub>2</sub>O-  
260 CaO-MgO-FeO-Fe<sub>2</sub>O<sub>3</sub>-Al<sub>2</sub>O<sub>3</sub>-SiO<sub>2</sub>-TiO<sub>2</sub>-H<sub>2</sub>O-CO<sub>2</sub>. *Journal of Petrology*, 29, 445-522.

261 Bindi, L., Welch, M.D., Bendeliani, A.A., and Bobrov, A.V. (2020) Si-rich Mg-sursassite  
262 Mg<sub>4</sub>Al<sub>5</sub>Si<sub>7</sub>O<sub>23</sub>(OH)<sub>5</sub> with octahedrally coordinated Si: A new ultrahigh-pressure hydrous phase.  
263 *American Mineralogist*, 105, 1432–1435.

264 Birch, F. (1947) Finite elastic strain of cubic crystals. *Physical Review*, 71, 809–824.

265 Bromiley, G.D., and Pawley, A.R. (2002) The high-pressure stability of Mg-sursassite in a model  
266 hydrous peridotite: a possible mechanism for the deep subduction of significant volumes of H<sub>2</sub>O.  
267 *Contribution to Mineralogy and Petrology*, 142, 714-723.

268 Cai, N., Kikegawa, T., and Inoue, T. (2018) Compressibility of the 23 Å phase under high pressure and  
269 high temperature. *Physic of the Earth and Planetary Interiors*, 283, 1-6.

270 Cai, N., Inoue, T., Fujino, K., Ohfuji, H., and Yurimoto, H. (2015) A possible new Al-bearing hydrous  
271 Mg-silicate (23 angstrom phase) in the deep upper mantle. *American Mineralogist*, 100, 2330-2335.

272 Chantel, J., Manthilake, G.M., Frost, D.J., Beyer, C., Boffa Ballaran, T., Jing, Z., and Wang, Y. (2016)  
273 Elastic wave velocities in polycrystalline Mg<sub>3</sub>Al<sub>2</sub>Si<sub>3</sub>O<sub>12</sub>-pyrope garnet to 24 GPa and 1300 K.  
274 *American Mineralogist*, 101, 991-997.

275 Chervin, J.C., Canny, B., and Mancinelli, M. (2001) Ruby-spheres as pressure gauge for optically  
276 transparent high pressure cells. *High Pressure Research*, 21, 305-314.

277 Comodi, P., Fumagalli, P., Montagnoli, M., and Zanazzi, P.F. (2004) A single-crystal study on the  
278 pressure behavior of phlogopite and petrological implications. *American Mineralogist*, 89, 647-653.

279 Comodi, P., Cera, F., Dubrovinsky, L., and Nazzareni, S. (2006) The high-pressure behaviour of the 10  
280 Å phase: a spectroscopic and diffractometric study up to 42 GPa. *Earth and Planetary Science Letters*,  
281 246, 444-457.

282 Crichton, W.A., Ross, N.L., and Gasparik, T. (1999) Equations of state of magnesium silicates anhydrous  
283 B and superhydrous B. *Physics and Chemistry of Minerals*, 26, 570-575.

284 Crichton, W.A., and Ross, N.L. (2000) Equation of state of phase E. *Mineralogical Magazine*, 64, 561-  
285 567.

286 Crichton, W.A., and Ross, N.L. (2002) Equation of state of dense hydrous magnesium silicate phase A,  
287  $Mg_7Si_2O_8(OH)_6$ . *American Mineralogist*, 87, 333-338.

288 Domanik, K.J., and Holloway, J.R. (1996) The stability and composition of phengitic muscovite and  
289 associated phases from 5.5 to 11 GPa: Implications for deeply subducted sediments. *Geochimica et*  
290 *Cosmochimica Acta*, 60, 4133-4150.

291 Fockenberg, T. (1998) An experimental study of the pressure-temperature stability of MgMgAl-  
292 pumpelleyite in the system MgO-Al<sub>2</sub>O<sub>3</sub>-SiO<sub>2</sub>-H<sub>2</sub>O. *American Mineralogist*, 83, 220-227.

293 Fumagalli, P., and Poli, S. (2005) Experimentally determined phase relations in hydrous peridotites to  
294 6.5 GPa and their consequences on the dynamics of subduction zones. *Journal of Petrology*, 46, 555-578.

295 Fumagalli, P., Poli, S., Fischer, J., Merlini, M., and Gemmi, M. (2014) The high-pressure stability of  
296 chlorite and other hydrates in subduction mélanges: experiments in the system Cr<sub>2</sub>O<sub>3</sub>-MgO-Al<sub>2</sub>O<sub>3</sub>-SiO<sub>2</sub>-  
297 H<sub>2</sub>O. *Contributions to Mineralogy and Petrology*, 167, 979.

298 Gatta, G.D., Merlini, M., Valdrè, G., Liermann, H.-P., Nénert, G., Rothkirch, A., Kahlenberg, V., and  
299 Pavese, A. (2013) On the crystal structure and compressional behavior of talc: a mineral of interest in  
300 petrology and material science. *Physics and Chemistry of Minerals*, 40, 145-156.

301 Gemmi, M., Merlini, M., Palatinus, L., Fumagalli, P., and Hanfland, M. (2016) Electron diffraction  
302 determination of 11.5 Å and HySo structures: Candidate water carriers to the Upper Mantle. *American*  
303 *Mineralogist*, 101, 2645-2654.

304 Gottschalk, M., Fockenberg, T., Grevel, K.-D., Wunder, B., Wirth, R., Schreyer, W., and Maresch, W.V.  
305 (2000) Crystal structure of the high-pressure phase  $Mg_4(MgAl)Al_4[Si_6O_{21}/(OH)_7]$ : an analogue of  
306 sursassite. *European Journal of Mineralogy*, 12, 93-945.

307 Grevel, K.-D., Navrotsky, A., Kahl, W.A., Fasshauer, D.W., and Majzlan, J. (2001) Thermodynamic data  
308 of the high-pressure phase  $Mg_5Al_5Si_6O_{21}(OH)_7$  (Mg-sursassite). *Physics and Chemistry of Minerals*, 28,  
309 475-487.

310 Hamilton, D.L., and Henderson, C.M.B. (1968) The preparation of silicate composition by gelling  
311 method. *Mineralogical Magazine*, 36, 832-838.

312 Hazen, R., and Finger, L. (1982) *Comparative crystal chemistry*, 231 p. Wiley, New York.

313 Holland, T.J.B., and Powell, R. (2011) An improved and extended internally consistent thermodynamic  
314 dataset for phases of petrological interest, involving a new equation of state for solids. *Journal of*  
315 *Metamorphic Geology*, 29, 333 - 383.

316 Klotz, S., Chervin, J-C, Munsch, P., and Le Marchand, G. (2009) Hydrostatic limits of 11 pressure  
317 transmitting media. *Journal of Physics D: Applied Physics*, 42, 075413.

318 Lotti, P., Milani, S., Merlini, M., Joseph, B., Alabarse, F., and Lausi, A. (2020) Single-crystal diffraction  
319 at the high-pressure Indo-Italian beamline Xpress at Elettra, Trieste. *Journal of Synchrotron Radiation*,  
320 27, 222-229.

321 Luth, R.W. (2003) Mantle Volatiles – Distribution and Consequences. In H.D. Holland and K.K.  
322 Turekian, Eds., *The Mantle and Core*, 2, p. 319-361. *Treatise on Geochemistry*. Elsevier Ltd.

323 Mao, H.K., Xu, J., and Bell, P.M. (1986) Calibration of the ruby pressure gauge to 800 kbar under quasi-  
324 hydrostatic conditions. *Journal of Geophysical Research*, 91, 4673-4676.

325 Merlini, M., and Hanfland, M. (2013) Single crystal diffraction at megabar conditions by synchrotron  
326 radiation. *High-Pressure Research*, 33, 511–522.

327 Momma, K., and Izumi, F. (2011) *VESTA 3* for three-dimensional visualization of crystal, volumetric  
328 and morphology data. *Journal of Applied Crystallography*, 44, 1272-1276.

329 Nagashima, M., Akasaka, M., Minakawa, T., Libowitzky, E., and Armbruster, T. (2009) Sursassite:  
330 hydrogen bonding, cation order, and pumpellyite intergrowth. *American Mineralogist*, 94, 1440–1449.

331 Nestola, F., Boffa-Ballaran, T., Balic-Zunic, T., Princivalle, F., and Dal Negro, A. (2007) Comparative  
332 compressibility and structure behavior of spinel  $MgAl_2O_4$  at high pressure: the independency on degree  
333 of cation order. *American Mineralogist*, 92, 1838-1843.

334 Nestola, F., Angel, R.J., Zhao, J., Garrido, C.J., López Sánchez-Viscaíno, V., Capitani, G., and Mellini,  
335 M. (2010) Antigorite equation of state and anomalous softening at 6 GPa: an in situ single-crystal X-ray  
336 diffraction study. *Contributions to Mineralogy and Petrology*, 160, 33-43.

337 Pawley, A.R., Clark, S.M., and Chinnery, N.J. (2002) Equation of state measurements of chlorite,  
338 pyrophyllite, and talc. *American Mineralogist*, 87, 1172-1182.

339 Petricek, V., Dusek, M., and Palatinus, L. (2014) Crystallographic Computing System JANA2006:  
340 General features. *Zeitschrift fur Kristallographie*, 229, 345-352.

341 Purevjav, N., Okuchi, T., and Hoffman, C. (2020) Strong hydrogen bonding in a dense hydrous  
342 magnesium silicate discovered by neutron Laue diffraction. *IUCrJ*, 7, 370-374.



343 Rigaku Oxford Diffraction, CrysAlisPro Software system, version 1.171.40.67a (2019), Rigaku  
344 Corporation, Wroclaw, Poland.

345 Ringwood, A.E. (1967) Pyroxene–garnet transition in the Earth’s mantle. *Earth and Planetary Science*  
346 *Letters*, 2, 255–263.

347 Schreyer, W., Maresch, W.V., Medenbach, O., and Baller, T. (1986) Calcium free pumpellyite, a new  
348 synthetic hydrous Mg-Al silicate found at high-pressures. *Nature*, 321, 510-511.

349 Smyth, J.R. (2006) Hydrogen in High Pressure Silicate and Oxide Mineral Structures. In H. Keppler and  
350 J.R. Smyth, Eds., *Water in Nominally Anhydrous Minerals*, 62, p 85-110. *Reviews in Mineralogy and*  
351 *Geochemistry*, Mineralogical Society of America, Chantilly, Virginia.

352 Tateiwa, N., and Haga, Y. (2009) Evaluations of pressure-transmitting media for cryogenic experiments  
353 with diamond anvil cell. *Review of Scientific Instruments*, 80, 123901.

354 van Keken, P.E., Kiefer, B., and Peacock, S.M. (2002) High-resolution models of subduction zones:  
355 Implications for mineral dehydration reactions and the transport of water into the deep mantle.  
356 *Geochemistry, Geophysics, Geosystems*, 3, 1056.

357 Welch, M.D., Gatta, G.D., and Rotiroti, N. (2011) The high-pressure behavior of orthorhombic  
358 amphiboles. *American Mineralogist*, 96, 623-630.

359

360 **Figure captions**

361 **Figure 1** (a) crystal structure of the Mg-sursassite projected parallel to [0 1 0], (b) as in (a) but  
362 superimposed are the Fourier-difference maxima close to O6, O7 and O11, where the H atoms are  
363 located. All the representations of the structure are realized using the program VESTA (Momma and  
364 Izumi 2011).

365 **Figure 2** Evolution of the unit-cell volume with pressure of the Mg-sursassite. The solid line represents  
366 the 2<sup>nd</sup> order BM-EoS fit.

367 **Figure 3** Evolution of the unit-cell volume with pressure of the natural sursassite. The solid line  
368 represents the 2<sup>nd</sup> order BM-EoS fit.

369 **Figure 4** Evolution of the unit-cell volume with temperature of the Mg-sursassite. Data were fitted with  
370 a Berman type EoS (solid line).

371 **Figure 5** Evolution of the density of Mg-sursassite along a *P-T* path representative of the top (solid  
372 line) and bottom (dashed line) of a cold subducting slab (based on the isoviscous model of van Keken  
373 et al. 2002). Thermodynamic data for forsterite (fo) are from Holland and Powell (2011). Mg-sursassite  
374 is indicated as Mg-surs. Density has been calculated using the equation of state for solids from Holland  
375 and Powell (2011).

376

377

**Table 1.** Major element composition (in wt%) of Mg-sursassite synthesised in this work. Each column represents the analysis of one crystal in the experimental charge.

SiO <sub>2</sub>	41.28	40.91	43.20	40.84	41.70	41.53	41.95	41.18	41.70	41.36
Al <sub>2</sub> O <sub>3</sub>	28.12	28.2	28.93	29.04	28.11	28.13	27.96	28.97	28.11	28.59
MgO	21.48	21.16	23.00	22.88	22.92	22.98	23.10	22.67	23.13	22.80
tot	90.88	90.27	95.12	92.77	92.73	92.64	93.02	92.82	92.95	92.74
(apfu)										
Si	6.21	6.19	6.19	5.99	6.12	6.10	6.14	6.04	6.10	6.07
Al	4.98	5.03	4.89	5.02	4.86	4.87	4.82	5.01	4.85	4.94
Mg	4.81	4.78	4.92	5.00	5.01	5.03	5.04	4.96	5.05	4.99
average										
Si	6.11(8)									
Al	4.93(8)									
Mg	4.96(10)									

378

379

**Table 2.** Details pertaining to the data collections and structure refinements of the Mg-sursassite studied in this work.

$a$ (Å)	8.5375(16)
$b$ (Å)	5.7097(11)
$c$ (Å)	9.6477(17)
$\beta$ (Å)	108.340(17)
$V$ (Å <sup>3</sup> )	446.40(15)
Space group	$P2_1/m$
$\lambda$ (Å)	0.71073
$\theta_{\max}$ (°)	27.18
No. measured reflections	5808
No. unique reflections	1053
No. refined parameters	124
No. restraints	0
$R_{int}$	0.0382
$R_1$ ( $F$ )	0.0306
$wR_2$ ( $F^2$ )	0.0412
GooF	1.83
Residuals (e <sup>-</sup> /Å <sup>3</sup> )	-0.44/+0.56

**Table 3.** Lattice parameters of Mg-sursassite at different pressures, collected using neon as  $P$ -transmitting medium ( $P$ -uncertainty:  $\pm 0.05$  GPa).

$P$ (GPa)	$a$ (Å)	$b$ (Å)	$c$ (Å)	$\beta$ (°)	$V$ (Å <sup>3</sup> )
0.001	8.508(4)	5.7158(4)	9.6498(9)	108.13(2)	445.98(17)
0.08	8.4910(2)	5.6849(3)	9.6012(4)	108.183(10)	445.88(1)
0.21	8.5275(7)	5.7023(1)	9.6398(2)	108.298(5)	445.05(15)
0.53	8.5221(9)	5.6977(1)	9.6305(2)	108.259(6)	444.07(15)
1.17	8.5060(2)	5.6921(3)	9.6156(4)	108.212(10)	442.26(13)
1.82	8.4910(2)	5.6849(3)	9.6012(4)	108.183(10)	440.34(12)
2.54	8.4744(10)	5.6778(2)	9.5866(2)	108.134(7)	438.32(13)
3.34	8.4538(7)	5.6663(1)	9.5632(2)	108.076(5)	435.48(15)
3.94	8.4409(4)	5.6600(1)	9.5504(1)	108.056(3)	433.81(10)
4.13	8.4373(4)	5.6583(1)	9.5470(1)	108.046(3)	433.35(10)
4.47	8.4306(5)	5.6551(1)	9.5398(2)	108.022(3)	432.50(12)
5.32	8.4132(6)	5.6461(1)	9.5217(2)	107.982(3)	420.20(12)
5.92	8.3997(6)	5.6395(1)	9.5079(2)	107.947(4)	428.48(12)
6.60	8.3840(8)	5.6305(1)	9.4907(2)	107.915(5)	426.30(13)
7.44	8.3670(2)	5.6255(2)	9.4778(4)	107.861(14)	424.61(12)
8.02	8.3540(2)	5.6175(2)	9.4624(4)	107.833(13)	422.73(19)
8.81	8.3430(2)	5.6118(2)	9.4509(4)	107.806(12)	421.26(12)
9.60	8.3260(2)	5.6031(2)	9.4334(4)	107.765(14)	419.09(11)
10.40	8.3100(2)	5.5940(2)	9.4163(4)	107.736(14)	416.94(11)
11.05	8.3000(2)	5.5871(2)	9.4027(4)	107.708(15)	415.38(12)
11.90	8.2860(2)	5.5801(2)	9.3891(4)	107.684(12)	413.6(12)
12.41	8.2780(3)	5.5752(3)	9.3788(5)	107.655(18)	412.48(12)
12.78	8.2760(2)	5.5734(2)	9.3758(4)	107.654(14)	412.09(11)
13.47	8.2561(9)	5.5612(1)	9.3551(2)	107.642(5)	409.33(15)
14.87	8.2379(9)	5.5515(1)	9.3364(2)	107.605(5)	406.98(14)
15.88	8.2246(13)	5.5439(1)	9.3224(2)	107.574(7)	405.23(19)

**Table 4.** Lattice parameters of Mg-sursassite at different temperatures, collected in a quartz vial ( $T$ -uncertainty:  $\pm 1$  K).

$T$ (K)	$a$ (Å)	$b$ (Å)	$c$ (Å)	$\beta$ (°)	$V$ (Å <sup>3</sup> )
317	8.5392(4)	5.7078(2)	9.6498(4)	108.324(4)	446.483(3)
342	8.5417(2)	5.7094(9)	9.6533(2)	108.333(2)	446.878(13)
372	8.5455(2)	5.7091(2)	9.6530(2)	108.352(2)	446.987(16)
401	8.5491(2)	5.7113(1)	9.6560(2)	108.365(2)	447.449(14)
431	8.5529(2)	5.7126(3)	9.6597(2)	108.376(2)	447.898(13)
460	8.5571(2)	5.7137(2)	9.6632(2)	108.382(2)	448.354(18)
490	8.5604(2)	5.7157(9)	9.6669(2)	108.394(2)	448.822(13)
519	8.5643(2)	5.7177(1)	9.6704(2)	108.403(2)	449.322(14)
549	8.5683(2)	5.7191(1)	9.6744(2)	108.412(2)	449.802(14)
578	8.5727(2)	5.7205(2)	9.6791(2)	108.418(2)	450.350(19)
608	8.5765(2)	5.7224(2)	9.6825(2)	108.429(3)	450.829(2)
638	8.5801(2)	5.7245(1)	9.6864(2)	108.439(2)	451.340(14)
667	8.5842(2)	5.7262(1)	9.6906(2)	108.447(2)	451.863(14)
697	8.5879(2)	5.7280(2)	9.6953(2)	108.459(2)	452.385(16)
726	8.5901(2)	5.7290(2)	9.6983(2)	108.464(2)	452.712(15)
756	8.5961(2)	5.7321(2)	9.7038(2)	108.469(2)	453.511(15)
785	8.6004(2)	5.7341(2)	9.7094(2)	108.473(2)	454.151(15)
815	8.6034(2)	5.7353(2)	9.7142(2)	108.467(2)	454.646(17)

383

384

**Table 5.** Thermo-elastic parameters of Mg-sursassite fitted by a Thermal pressure model (Holland and Powell 2011).

$V_0$ ( $\text{\AA}^3$ )	$K_{T0}$ (GPa)	$K'$	$\alpha_0$ ( $\times 10^{-5} \text{ K}^{-1}$ )	Reference
446.00(5)	135.5(9)	4	2.95(4)	This work
446.25(15)	120.03	4	2.74(8)	Grevel et al. (2001)

**Table 6.** Comparison of bulk moduli of Mg-sursassite and other hydrous and anhydrous phases in MASH system.

Mineral	$K_{T0}$ (GPa)	$K'$	$V_0$ ( $\text{\AA}^3$ )	EoS	Reference
Mantle olivine	126.3(2)	4.54(5)	291.5	BM III	Angel et al. (2018)
orthoenstatite	105.7(1.9)	8.4(6)	832.5(2)	BM III	Angel and Jackson (2002)
antophyllite	65.8(1.6)	10.5(1.1)	1766.07(3)	BM III	Welch et al. (2011)
pyrope	170.8(1.5)	4.43(8)	-	BM III	Chantel et al. (2016)
spinel	192(1)	5.4(3)	528.39(2)	BM III	Nestola et al. (2007)
talc	56(3)	5.4(7)	454.7(10)	BM III	Gatta et al. (2013)
phlogopite	54(2)	7(1)	497.1(1)	BM III	Comodi et al. (2004)
antigorite	62.9(4)	6.1(2)	2914.07(23)	BM III	Nestola et al. (2010)
chlorite	89.5(3)	4	699.2	BM II	Pawley et al. (2002)
Mg-sursassite	135.6(7)	4	446.01(10)	BM II	This study
11.5 $\text{\AA}$ phase	108.3(2)	4	1066.53(2)	BM II	Gemmi et al. (2016)
23 $\text{\AA}$ phase	111(1)	4	538.0(3)	BM II	Cai et al. (2018)
HySo	120.6(6)	4	676.8(3)	BM II	Gemmi et al. (2016)
10 $\text{\AA}$ phase	39(3)	12.5(8)	492.9(3)	BM III	Comodi et al. (2006)
phase A	97.5(4)	5.97(14)	512.56(3)	BM III	Crichton and Ross (2002)
Shy-B	142.6(8)	5.8(2)	624.71(3)	BM III	Crichton et al. (1999)
phase E	92.9(7)	7.3(2)	105.627(7)	BM III	Crichton and Ross (2000)
Anhy-B	151.5(9)	5.5(3)	838.86(4)	BM III	Crichton et al. (1999)



Figure 1

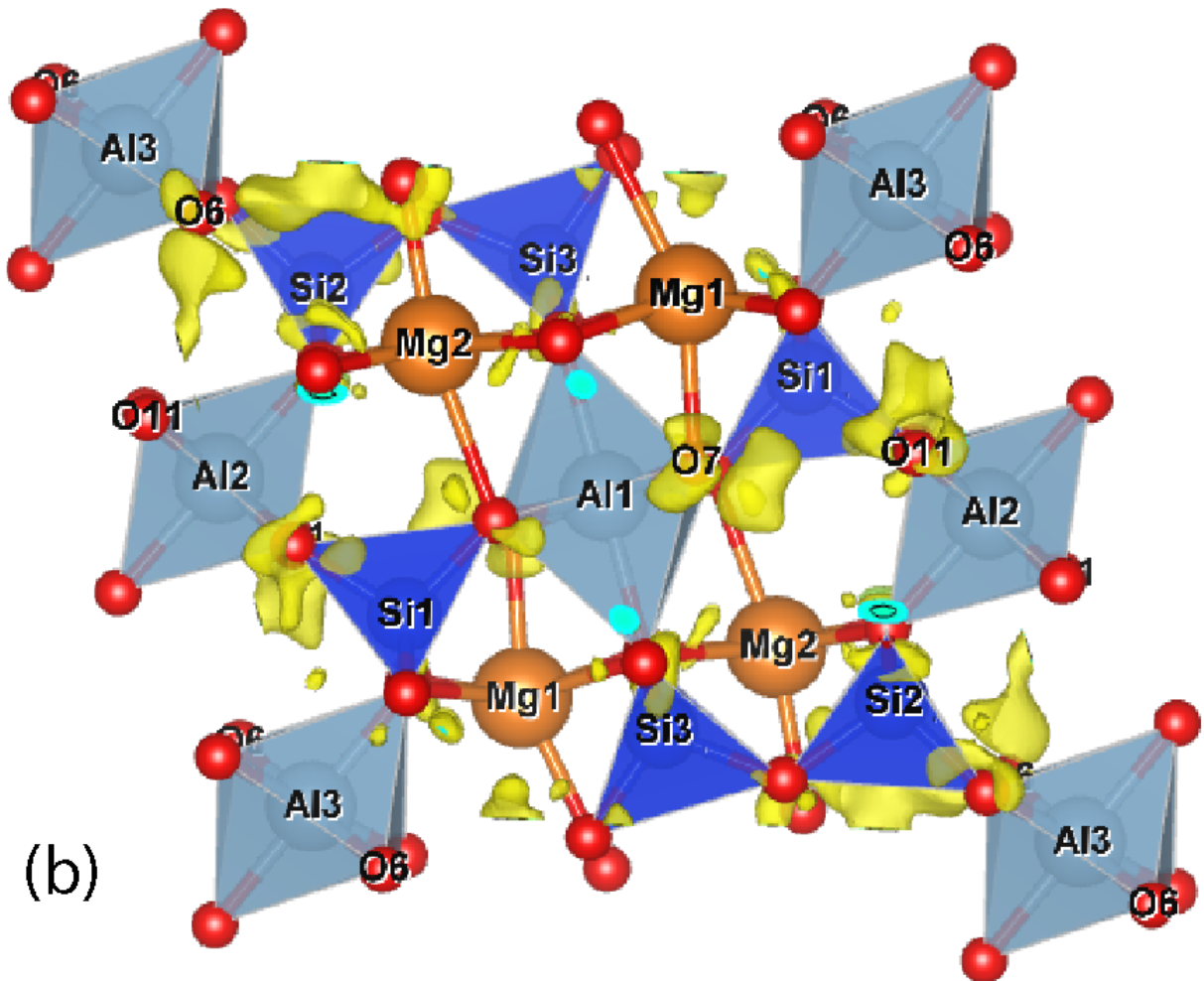
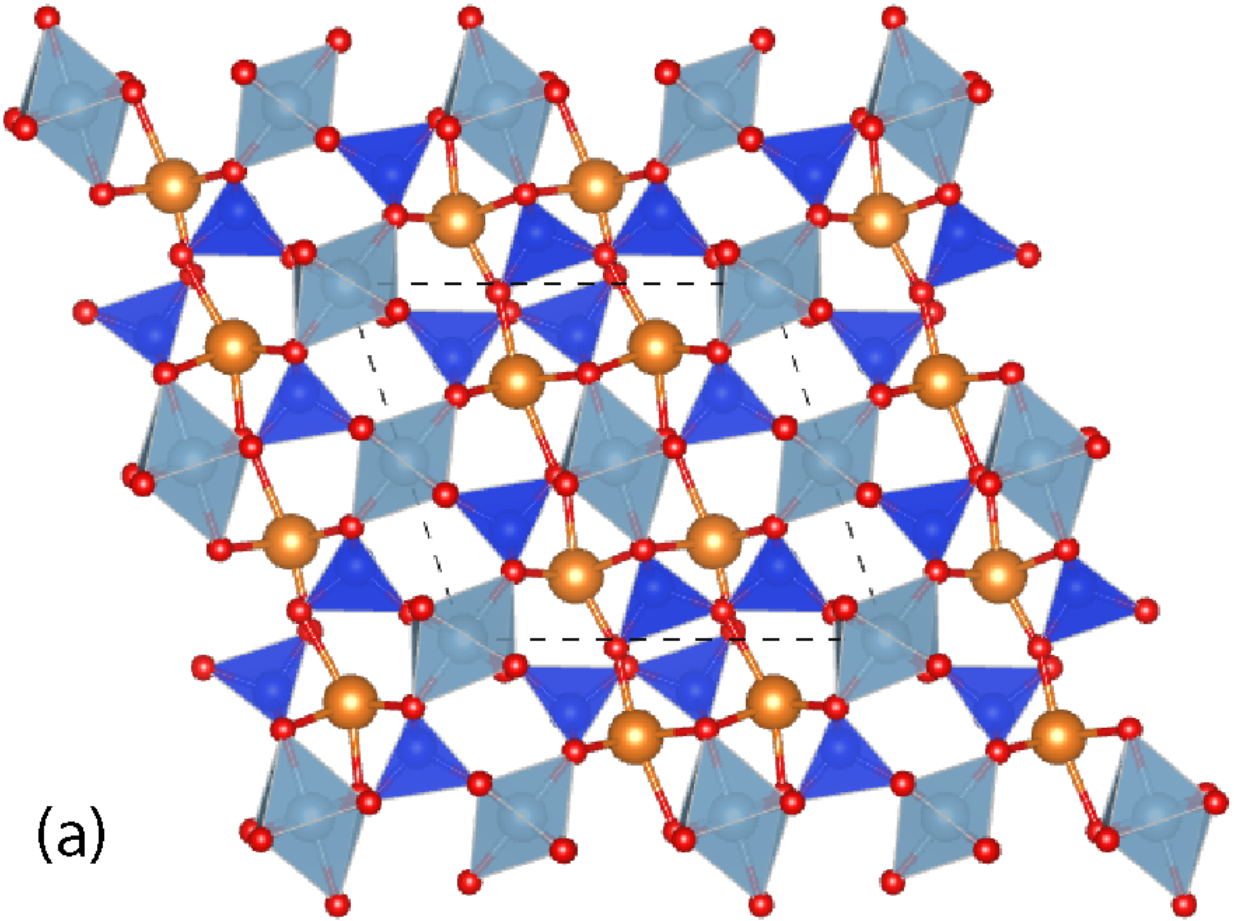


Figure 2

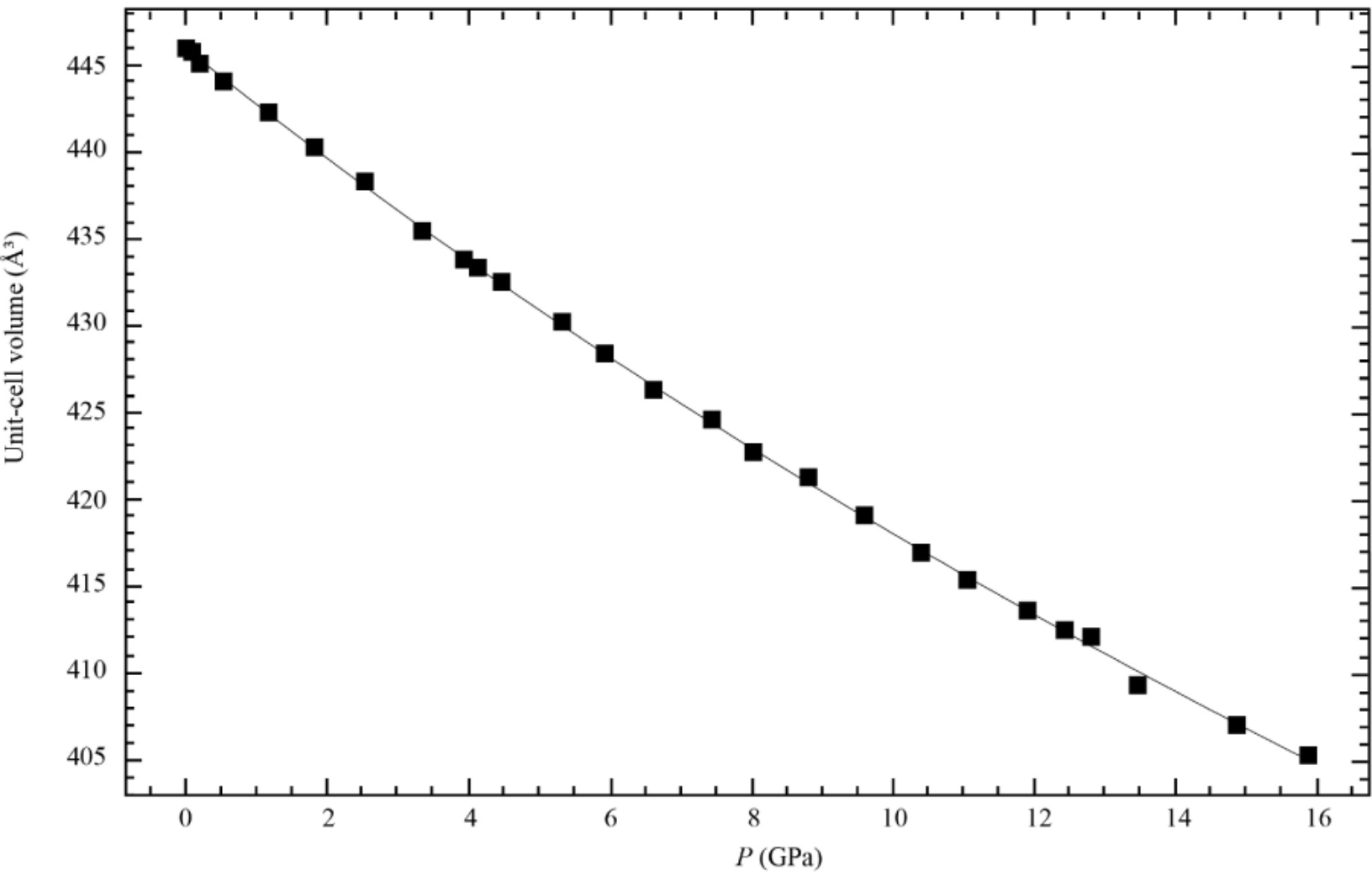
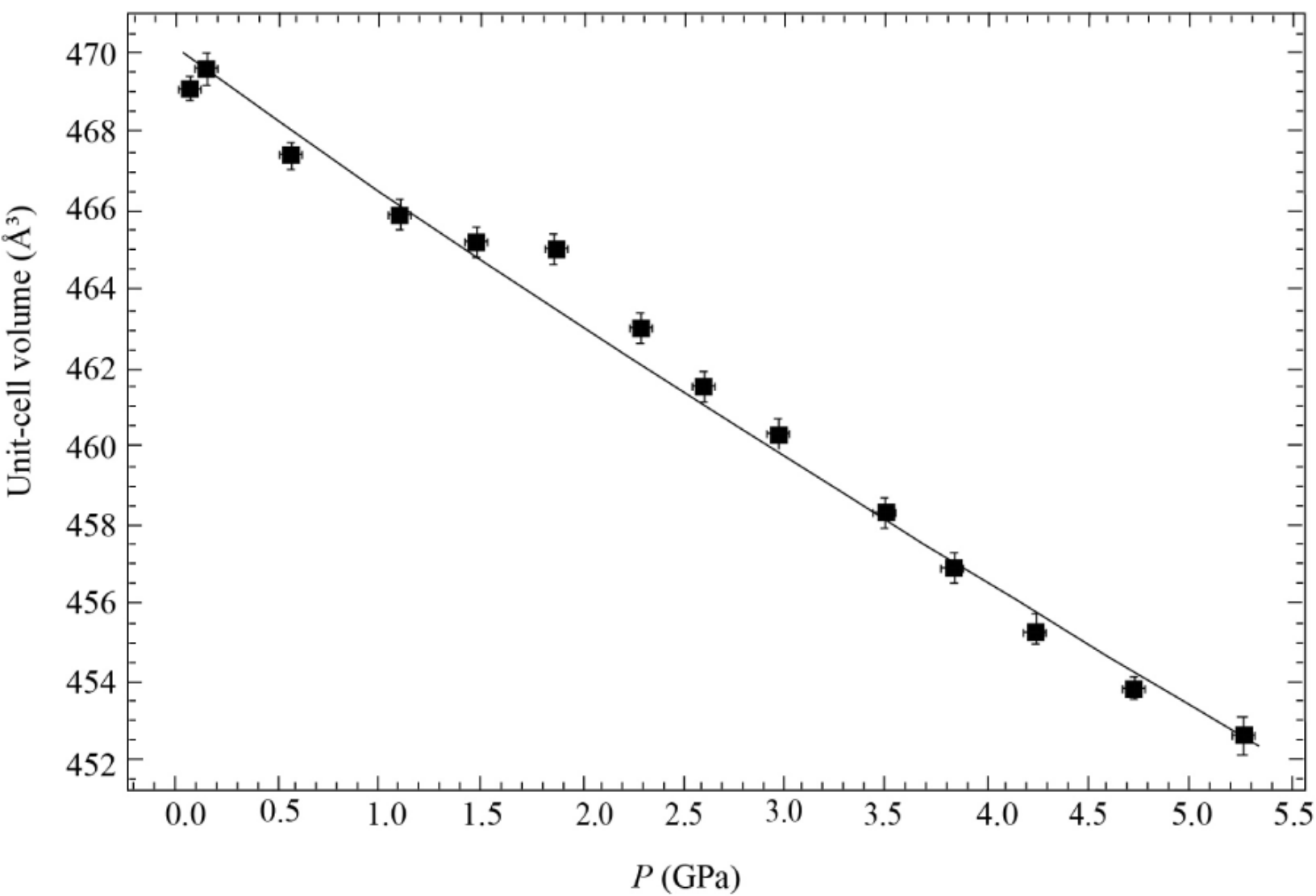


Figure 3



# Figure 4

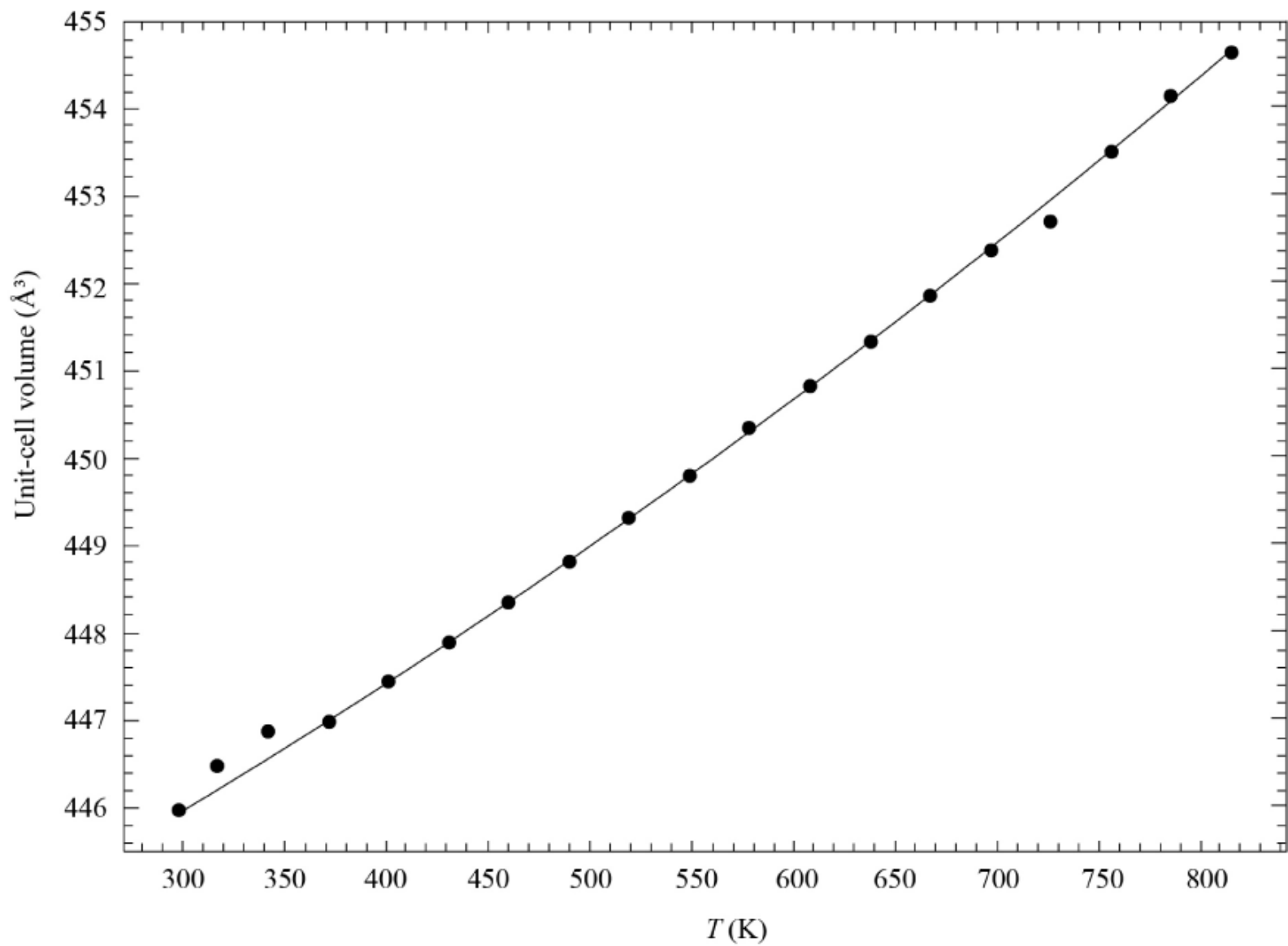


Figure 5

